ponents fixed at 1.80. An exponent of 1.16 was used for the H 1s atomic orbital.

Single-Crystal X-ray Structural Determinations. General operating procedures and listings of programs have been described.[24] A summary of crystal data is given in Table II. Full details are provided in the supplementary materials.

Acknowledgment. We thank the National Science Foundation for support and Professors John Verkade and Odile Eisenstein for valuable discussion. We also note that the compound $W_2(\mu\text{-}PPh_2)_2(O\text{-}t\text{-}Bu)_4$ reported in this paper was first prepared by Professor Bryan Eichhorn (current address: Department of Chemistry, The University of Maryland, College Park, MD 20742).

Registry No. 1a, 137566-81-5; **1g**, 106651-38-1; **2a**, 137566-82-6; **2b**, 110303-35-0; **2g**, 116212-37-4; **3a**, 137467-40-4; **3b**, 137467-41-5; **3g**, 137566-74-6; **4a**, 137467-42-6; **4g**, 137566-75-7; **5a**, 137467-43-7; **5b**, 137467-44-8; **5g**, 137566-76-8; **6a**, 137467-45-9; **6b**, 137467-46-0; **6g**, 137566-77-9; **7a**, 137467-47-1; **7b**, 137467-48-2; **7g**, 137566-78-0; **8**, 137567-64-7; **8a**, 137467-49-3; **8g**, 137566-79-1; **9**, 137567-65-8; **9a**, 137467-31-3; **9g**, 137566-65-5; **10g**, 137467-32-4; **11a**, 137467-33-5; **11g**, 137566-66-6; **12a**, 137566-67-7; **12b**, 116301-30-5; **12g**, 137566-68-8; **13a**, 137566-69-9; **13b**, 116301-31-6; **13g**, 137566-70-2; **14a**, 137467-34-6; **14g**, 137566-71-3; **15a**, 137467-35-7; **15g**, 137566-72-4; **16a**, 137467-36-8; **16g**, 137566-73-5; **17a**, 137467-37-9; **17g**, 137567-66-9; **18**, 137495-96-6; **19b**, 137467-38-0; *anti*-1,2-$Mo_2(P(t\text{-}Bu)_2)_2(NMe_2)_4$, 106651-37-0; *gauche*-1,2-$Mo_2(P(t\text{-}Bu)_2)_2(NMe_2)_4$, 137566-80-4; 1,2-$W_2Cl_2(NMe_2)_4$, 63301-81-5; $W_2(\mu\text{-}PPh_2)_2(O\text{-}t\text{-}Bu)_4$, 110303-34-9; Mo, 7439-98-7; W, 7440-33-7; $W_2(\mu\text{-}PH_2)_2(NH_2)_4$, 137467-39-1.

Supplementary Material Available: Listings of h, k, l, F_o, and F_c values for $Mo_2(P(t\text{-}Bu)_2)_2(NMe_2)_4$, *anti*-$W_2(P(t\text{-}Bu)_2)_2(NMe_2)_4$, *gauche*-$W_2(P(t\text{-}Bu)_2)_2(NMe_2)_4$, $W_2(P(cyclohexyl)_2)_2(NMe_2)_4$, $W_2(P(SiMe_3)_2)_2(NMe_2)_4$, and $W_2(P(C_6H_{11})_2)(P(SiMe_3)_2)(NMe_2)_4$ (56 pages). Ordering information is given on any current masthead page.

(24) Chisholm, M. H.; Folting, K.; Huffman, J. C.; Kirkpatrick, C. C. *Inorg. Chem.* **1984**, *23*, 1021.

A Molecular Dynamics Study of the Stability of Chymotrypsin Acyl Enzymes

Guy W. Bemis, Gail Carlson-Golab, and John A. Katzenellenbogen*

Contribution from the Department of Chemistry, University of Illinois, 1209 West California Street, Urbana, Illinois 61801. *Received June 17, 1991*

Abstract: We have investigated the enantioselectivity observed in the deacylation rates of a β-substituted β-phenylpropionyl chymotrypsin acyl enzyme by molecular dynamics simulations. The ca. 60-fold difference in deacylation rates for the *R* and *S* esters ($k_d(S) = 0.17$ min^{-1}; $k_d(R) = 0.0029$ min^{-1}) is presumed to derive from less optimal stabilization of reactive intermediates in the case of the *R* enantiomer. Structures for both *R* and *S* acyl enzymes were constructed starting from the X-ray structure of chymotrypsin phenylethaneboronic acid complex. The ester carbonyl oxygen was placed in the oxyanion binding hole (backbone NH's from Gly-193 and Ser-195), and the phenyl group was placed in the hydrophobic cleft. Structures corresponding to acyl enzymes in which the β-substituent, an acetonyl chain, was engaged in hydrogen bonding with seven possible hydrogen bond donors near the active site were generated. Only three of these (Met-192 NH, Gly-216 NH, and Ser-218 OH) survived rigorous molecular mechanics minimization, and these three structures, in both the *R* and *S* acyl enzyme series, were subjected to molecular dynamics. In all three *R* acyl enzymes, the crucial hydrogen interaction between the ester carbonyl oxygen and the oxyanion binding hole was weakened during the dynamics run, whereas in two of the three *S* acyl enzymes, these hydrogen bonds persisted. There was also some rearrangement of the hydrogen-bonding configuration for the acetonyl side chain. An additional molecular dynamics study was done on the tetrahedral intermediates corresponding to the deacylation of the *R* and *S* acyl enzymes. Although, as expected, the hydrogen-bonding interaction between the oxyanion in the tetrahedral intermediate and the hydrogen bond donors in the oxyanion binding hole was strengthened for both enantiomers, the *R* enantiomer showed less ideal stabilization. These results provide a rationalization for the deacylation enantioselectivity of these acyl enzymes: The reduced deacylation rate of the *R* enantiomer could arise from less effective hydrogen-bonding stabilization of both the ester carbonyl in the acyl enzyme and the oxyanion in the deacylation tetrahedral intermediate by the oxyanion binding hole site; the *S* enantiomer, which preserves excellent hydrogen bond distances and geometry at both stages, is more ideally set up for the attack of water that leads to deacylation.

Introduction

The prodigious catalytic activity of serine proteases and their substrate specificity have long fascinated researchers. More recently, certain proteases of this class have become targets for the development of potent, selective inhibitors that might prove to have therapeutic utility.[1] A clearer understanding of the structural and stereochemical factors that control the stability of the various intermediates in the serine protease-catalyzed hydrolysis pathway would assist in the development of such inhibitors. Nevertheless, despite a clear general understanding of the specificity interactions[2] and major functional features involved in the hydrolysis process,[3] and despite many crystallographic studies on free proteases, as well as those complexed with both small and macromolecular complexes,[4] there has been little success in predicting how particular substrates and inhibitors will interact with protease active sites.

(1) For general references on the medical importance of protease inhibitors, see: (a) Rich, D. H. In *Comprehensive Medicinal Chemistry. The Rational Design, Mechanistic Study and Therapeutic Applications of Chemical Compounds*; Hansch, C., Sammes, P. G., Taylor, J. B., Eds.; Pergamon: New York, 1990. (b) *Design of Enzyme Inhibitors as Drugs*; Sandler, M., Smith, H. J., Eds.; Oxford University: Oxford, 1989. (c) *Proteases. Potential Role in Health and Disease*; Hörl, W. H., Heidland, E., Eds.; Plenum: New York, 1984.

(2) Segal, D. M.; Powers, J. C.; Cohen, G. H.; Davies, D. R.; Wilcox, P. E. *Biochemistry* **1971**, *10*, 3728-3738.

(3) Kraut, J. *Annu. Rev. Biochem.* **1977**, *46*, 311-358.

(4) These structures are available from the Brookhaven Protein Data Bank.

0002-7863/92/1514-570$03.00/0

Scheme I. Serine Protease Hydrolysis Mechanism

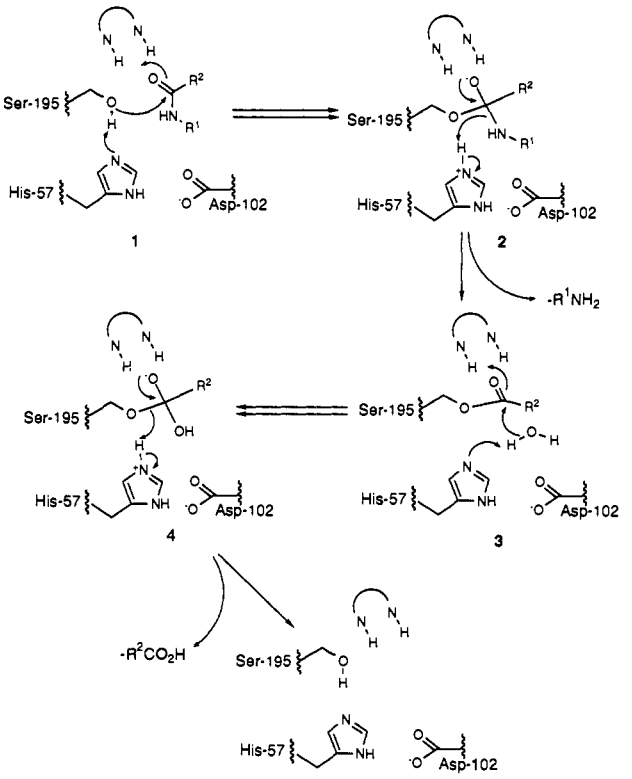

Hydrolysis of ester or amide substrates by serine proteases (Scheme I) involves acylation of the nucleophilic Oγ of Ser-195 (the nucleophilic element in the Asp-102/His-57/Ser-195 catalytic triad), followed by general-base-assisted hydrolysis of the acyl enzyme intermediate. For amide substrates, the rate-limiting step is **1** → **2** whereas for esters it is **3** → **4**. The high-energy transition states leading to and from the high-energy tetrahedral intermediates are stabilized by hydrogen-bonding interaction with two backbone NH's of Ser-195 and Gly-193, which together constitute the oxyanion binding hole. For chymotrypsin, the aromatic residue projects into a hydrophobic cleft.

Previous theoretical studies by DeTar[5] and Wipff[6] have focused on analyzing the relative rates for α-chymotrypsin[7] catalyzed hydrolysis of the enantiomers of *N*-acetyltryptophanamide substrates, using molecular mechanics to model the active site of α-chymotrypsin for the acylation tetrahedral intermediates **2**. Both studies suggest that a hydrogen bond between the acetyl NH group and the carbonyl of Ser-214 is an important determinant of enantioselectivity.

In connection with our work on the development of enol lactone inhibitors and inactivators of serine proteases, we found that certain lactone substrates were effective inhibitors of chymotrypsin of the alternate substrate type;[8] i.e., these species inhibited the enzyme by forming an acyl enzyme intermediate that was stable and whose hydrolysis to complete the catalytic cycle was slow. These systems are chiral, and in a number of cases, we found considerable differences in the deacylation rate of the enantiomers.[8c] For example, the β-substituted β-phenylpropionic esters **7** and **8**, generated through acylation of chymotrypsin by lactones **5** and **6** (Scheme II) show enantioselectivity for the deacylation process by a factor of ca. 60, the *S* ester having a k_d of 0.17 min^{-1}, vs the *R* ester having a k_d of 0.0029 min^{-1}.[8b,c] Many of the errors

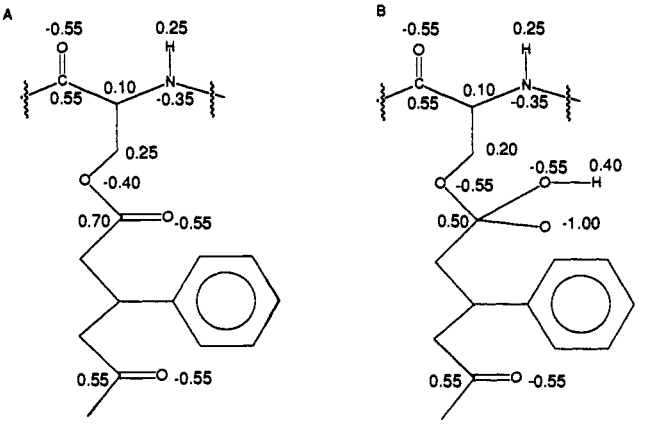

Figure 1. Partial charges used for acylated serine residue (A) and deacylation tetrahedral intermediate (B). Charge is 0.0 unless otherwise labeled.

encountered in quantitative molecular modeling of enzyme interaction with substrates of different structure are avoided by comparison of the interaction of enantiomers at the chiral binding site; therefore, we selected these esters for study. We chose to use molecular mechanics minimization followed by molecular dynamics simulation to examine the possible conformations for acyl enzymes **7** and **8** and their corresponding deacylation tetrahedral intermediates. By observing the time evolution of these systems, we hoped to be able to rationalize the specific kinetic data, and also to gain some insight into the complex problem of protein/ligand interactions.

Results and Discussion

Development of the Acyl Chymotrypsin Structural Models (7 and 8). Building the Active Site. To build the acyl enzyme structures **7** and **8** in α-chymotrypsin, we started from the crystal structure of phenylethaneboronic acid bound to α-chymotrypsin,[9] because the phenyl group of this inhibitor maintains the geometry of the hydrophobic pocket necessary for building our structures with a minimum of distortion. All calculations were performed on a Silicon Graphics 4D/25G, 4D/50G, or 4D/240S computer using version 2.1A of the Quanta program and version 21.1.7b of the CHARMM[10] program with parameters from the file PARM21A. Molecule A of the protein dimer and 95 crystallographic water molecules associated with it were selected, and molecule B with its water molecules was removed due to excessive disorder of the phenylethaneboronic acid.[9] Residues 9–13 (Val-Leu-Ser-Gly-Leu), which are not visible in the crystal structure electron density map, were constructed and minimized while holding the rest of the enzyme rigid. These residues are well separated from the active site, and their disorder in the crystal structure indicates their placement and motion have minimal effect on our calculations. Polar hydrogens were added to the enzyme, the phenylethaneboronic acid inhibitor was excised, and the complete set of amino acid side chains were minimized while the peptide backbone and crystallographically determined water oxygens were held rigid.

Defining New Residues. Residue topology files (RTF's) for two new serine residues were defined: one acylated with the *R* β-phenyl moiety and the other with the *S*. The charges for these new residues were computed on the basis of charges from very similar molecules in the standard CHARMM/quanta amino acid topology files: backbone charges were based on serine, ester charges on a methyl ester patch, phenyl ring charges on phenylalanine, and ketone charges on statone. Figure 1 shows charges used for both the *R* and the *S* acyl serine residues.

Normal Acyl Enzyme Structure Generation. The van der Waals interactions provided by the hydrophobic pocket of α-chymotrypsin are an important stabilizing feature for α-chymotrypsin acyl

(5) DeTar, D. F. *J. Am. Chem. Soc.* **1981**, *103*, 107.
(6) Wipff, G.; Dearing, A.; Weiner, P. K.; Blaney, J. M.; Kollman, P. A. *J. Am. Chem. Soc.* **1983**, *105*, 997.
(7) Chymotrypsinogen numbering system has been adopted. Chymotrypsin is EC 3.4.21.1.
(8) (a) Sofia, M. J.; Katzenellenbogen, J. A. *J. Med. Chem.* **1986**, *29*, 230–238. (b) Baek, D.-J.; Reed, P. E.; Daniels, S. B.; Katzenellenbogen, J. A. *Biochemistry* **1990**, *29*, 4305–4311. (c) Reed, P. E.; Katzenellenbogen, J. A. *J. Med. Chem.* **1991**, *34*, 1162–1176.
(9) Tulinsky, A.; Blevins, R. A. *J. Biol. Chem.* **1987**, *262*, 7737.
(10) Brooks, B. R.; Bruccoleri, R. E.; Olafson, B. D.; States, D. J.; Swaminathan, S.; Karplus, M. *J. Comput. Chem.* **1983**, *4*, 187–217.

Scheme II. Differential Hydrolysis Behavior for Lactones **5** and **6**

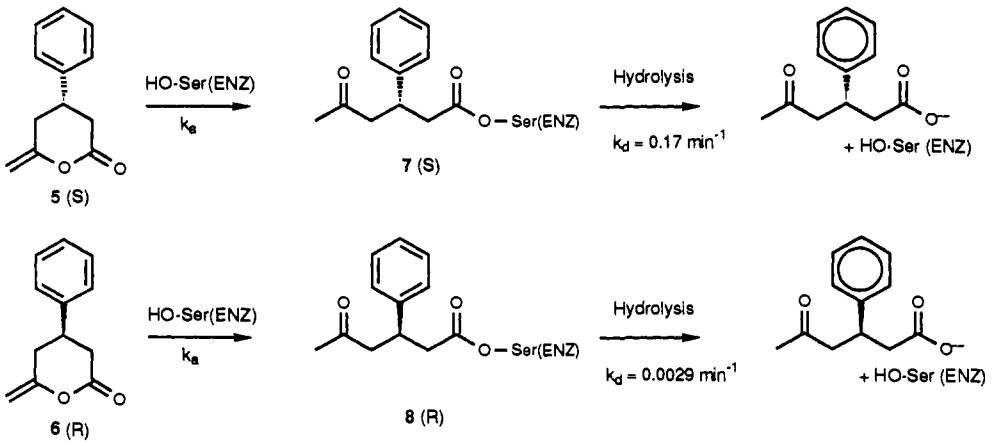

Scheme III. Carbonyl Exchange Process for Chymotrypsin Acyl Enzyme

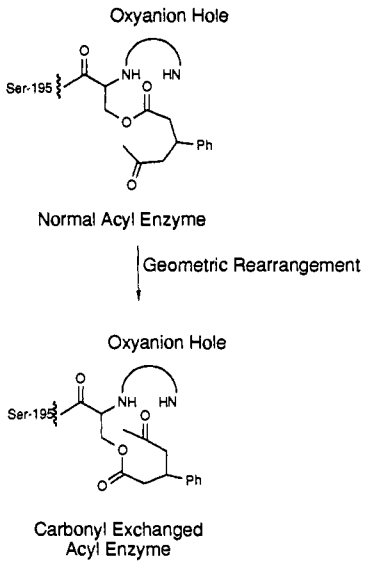

enzymes. It is therefore a reasonable assumption that the phenyl groups of the acyl enzymes **7** and **8** are bound in the hydrophobic pocket. In addition to this largely hydrophobic interaction, hydrogen bonding between the acyl side chain and the active site of α-chymotrypsin is an important factor in determining both the geometry and the stability of the acyl enzyme. Acylation of the serine residue should leave the ester carbonyl oxygen in or near the oxyanion binding hole. The difference between hydrocinnamoyl α-chymotrypsin, a "good" acyl enzyme, and the acyl enzymes we are studying, is the presence of an acetonyl group, as is demonstrated graphically in Scheme II.

Hydrogen Bond Donors. The largest effect of the acetonyl group in reducing the rate of deacylation is likely to be due to hydrogen bonding, if that is a geometric possibility.[11] Inspection of the active site of chymotrypsin reveals several hydrogen bond donors that are available for bonding to the ketone carbonyl oxygen of the acyl side chain. The possible donors are Tyr-146 (OH), Met-192 (NH), Ser-214 (NH), Trp-215 (NH), Gly-216 (NH), Ser-218 (OH), and Cys-220 (NH). An attempt was made to construct (using molecular mechanics tools) acyl enzymes for both the *R* and the *S* esters corresponding to each hydrogen-bonding pattern, with one of these seven residues as the hydrogen bond donor and the acetonyl ketone oxygen as the acceptor. The principal structural features of these acyl enzymes were as before (a) placement of the β-phenyl group in the hydrophobic pocket, (b) placement of the ester carbonyl oxygen close to both the Gly-193 and Ser-193 NH's (the oxyanion binding hole), and now (c) placement of the ketone carbonyl oxygen within approximately 4 Å of the potential hydrogen bond donor. Next, distance constraints were placed on the three hydrogen bonds (the two from the oxyanion binding hole to the ester carbonyl oxygen and the third, in turn, from each of the seven potential hydrogen bond donors in or near the active site to the acetonyl carbonyl oxygen). By constraining these distances to 2.87 Å, and minimizing the acyl side chain and the entire Ser-195 residue while holding the rest of the enzyme rigid (200 cycles of steepest descent + 200 cycles of adopted basis Newton Raphson (ABNR)), we eliminated distortions that may have resulted from the initial crude hand fitting of the hydrogen-bonded structures. The next minimization (500 cycles of ABNR) allowed all amino acid side chains to move freely, but kept the original distance constraints and held the protein backbone rigid. A final minimization (500 cycles of ABNR) was performed after the removal of all constraints. The particular hydrogen-bonding pattern being probed in each case was considered further only if the acyl side chain ketone carbonyl remained within reasonable hydrogen-bonding distance (4 Å) of the potential hydrogen bond donor during the last minimization sequence.

Only three hydrogen bond donors in the active site met all of these criteria; these were the NH of Met-192, the NH of Gly-216, and the OH of Ser-218. The remaining four, in both the *R* and *S* cases, minimized to structures in which the acetonyl ketone oxygen and the donor heteroatom were separated by more than 4 Å. In the stable structures that were found for these three hydrogen bond geometries for both the *R* and the *S* acyl enzymes, the ester carbonyl remained in the oxyanion binding hole, and the

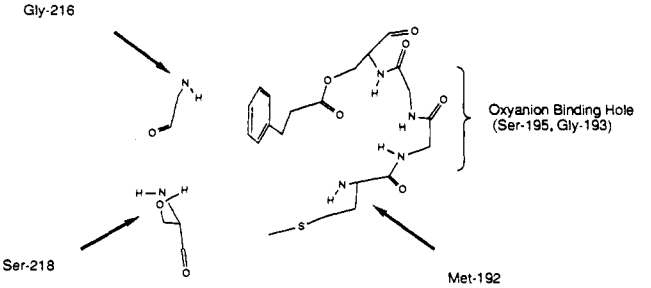

Figure 2. Schematic representation of chymotrypsin active site showing three potential hydrogen bond donors. Acyl enzyme is shown without acetonyl side chain.

(11) A number of force fields have a separate optional term that attempts to reproduce the conformational bias introduced by hydrogen bonding: (a) Brooks, B. R.; Bruccoleri, R. E.; Olafson, B. D.; States, D. J.; Swaminathan, S.; Karplus, M. *J. Comput. Chem.* **1983**, *4*, 187–217. (b) Vedani, A.; Dunitz, J. D. *J. Am. Chem. Soc.* **1985**, *107*, 7653. (c) Levitt, M. *J. Mol. Biol.* **1983**, *168*, 595. These terms include various representations of the distance between and angular disposition of donor and acceptor. However, because hydrogen bonding is largely electrostatic in nature, we used one of the best representations of this phenomenon that is provided by E_{elec}, the electrostatic energy term. (d) Hagler, A. T.; Huler, E.; Lifson, S. *J. Am. Chem. Soc.* **1974**, *96*, 5319. (e) McGuire, R. F.; Momany, F. A.; Scheraga, H. A. *J. Phys. Chem.* **1972**, *76*, 375.

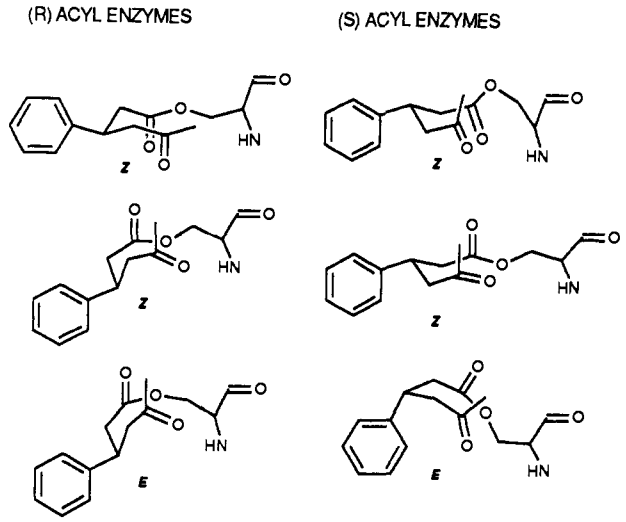

Figure 3. Geometry of starting structures for carbonyl-exchanged acyl enzymes.

Table I. Energies and Hydrogen Bond Distances for Minimized Acyl Enzymes

(stereochem) H bond donor	H bond distance (Å)	minimized energy (kcal/mol)	oxyanion hole distances (Å) Gly-193	Ser-195
Normal Acyl Enzymes				
(*R*) Met-192 NH	2.79	−5254.5	3.73	2.89
(*R*) Gly-216 NH	2.74	−5284.2	3.54	2.81
(*R*) Ser-218 OH	2.85	−5239.8	2.90	2.87
(*S*) Met-192 NH	2.85	−5180.3	3.10	2.86
(*S*) Gly-216 NH	2.88	−5342.6	2.86	2.74
(*S*) Ser-218 OH	2.84	−5178.0	2.78	2.76
Carbonyl-Exchanged Acyl Enzymes				
(*R*) *Z* ester		−5237.8	3.06	3.01
(*R*) *E* Ester		−5202.2	2.99	2.96
(*S*) *Z* Ester		−5189.0	2.90	3.01

phenyl group remained in the hydrophobic pocket. An indication of the geometric disposition of these hydrogen bond donors in the active site of chymotrypsin is shown in Figure 2.

Carbonyl-Exchanged Acyl Enzymes. We also examined the nature of carbonyl-exchanged acyl enzymes, that is, acyl enzymes in which the ketone carbonyl has replaced the ester carbonyl group in the oxyanion binding hole.[12] Such exchanged structures would be expected to be relatively inert toward deacylation, as the ester carbonyl group is displaced from the activating influence of the hydrogen bond donors of the oxyanion binding sites. Scheme III shows this exchange graphically.

Starting carbonyl-exchanged structures considered were in two classes; those with the ester bond in an *E* configuration and those with the more stable *Z* configuration.[13] For the initial phase of building these acyl enzymes, the ketone carbonyl oxygen was constrained to be in the oxyanion binding hole instead of the ester carbonyl oxygen. The ester carbonyl oxygen was first manually placed in the desired conformation, minimized with distance constraints to both the Gly-193 nitrogen and the Ser-195 nitrogen, and then minimized without constraints. Within these two classes, *E* esters and *Z* esters, starting structures were limited to three for the *R* acyl enzymes and three for the *S*, because of the geometric constraints imposed by the phenyl group/hydrophobic pocket interaction. Figure 3 gives a simplified picture of the starting geometries for the acylated Ser-195 residue in the twisted acyl enzymes. Table I shows energies and key distances for the fully minimized acyl enzymes that were selected for further consideration by the process described above.

(12) Naruto, S.; Motoc, I.; Marshall, G. R.; Daniels, S. B.; Sofia, M. J.; Katzenellenbogen, J. A. Unpublished work.

(13) Simonetta, M.; Carra, S. In *The Chemistry of Carboxylic Acids and Esters*; Patai, S., Ed.; John Wiley and Sons Ltd.: New York, 1969; p 14.

Table II. Averages for 20-ps Dynamics Simulation[a]

ketone H bond starting geometry	av simulatn potentl energy (kcal/mol)	av simulatn total energy (kcal/mol)	av simulatn temp (K)
R Met-192 NH	−4674.51 (566.67)	−2668.01 (0.97)	300.56 (4.10)
R Gly-216 NH	−4813.70 (561.66)	−2800.03 (0.79)	301.63 (3.49)
R Ser-218 OH	−4864.34 (516.41)	−2860.81 (0.72)	300.11 (3.51)
S Met-192 NH	−4702.94 (561.08)	−2708.94 (0.82)	298.68 (3.77)
S Gly-216 NH	−4726.78 (572.37)	−2709.60 (0.73)	302.16 (3.69)
S Ser-218 OG	−4746.28 (608.78)	−2736.46 (0.94)	301.05 (3.76)

[a] Numbers in parentheses are rms values.

Table III. Summary of Significant Hydrogen Bond Changes during Dynamics

		Met-192	Gly-216	Ser-218	Gly-193	Ser-195
R acyl enzymes						
	start	+			+	+
	finish	+			−	−
	start		+		+	+
	finish		+		−	−
	start		−	+	+	+
	finish		+	−	−	−
S acyl enzymes						
	start	+	−	−	+	+
	finish	−	+	+	−	−
	start		+	−	+	+
	finish		+	+	+	+
	start		−	+	+	+
	finish		+	−	+	+

Structures of Acyl Enzymes. Stereo ball and stick structures for acyl enzymes with the Gly-216 hydrogen bond are shown in Figure 4.

For both the *R* and the *S* acyl enzymes, the most stable minimized structures are those with the ketone carbonyl hydrogen bonded to the NH to Gly-216. Additionally, the ester carbonyl oxygens for most of the structures remain within hydrogen-bonding distance for both the Gly-193 and Ser-195 NH's.

Molecular Dynamics on Acyl Enzymes. The Verlet integration method was used to solve the equations of motion. The SHAKE algorithm was used to hold hydrogen/heteroatom bonds at a fixed length; consequently, we were able to use a time step (integration increment) of 0.001 ps. A distance-dependent dielectric was used; the $1/r^2$ term provides for rather quick cutoff of electrostatic interactions, and simplifies calculations. The merits of different forms for the electronic energy term have been discussed.[14]

Initial velocities were assigned on the basis of a Gaussian distribution and were rescaled, when necessary, by using a single-factor multiplication. The list of nonbonded interactions was regenerated every 25 time steps, with atom pairs included to a 10.5-Å radius. The van der Waals energy term was switched off over the range 9.5–10.0 Å, and the electrostatic term was switched off at 10 Å.

Heating. The acyl enzymes were heated from 0 to 300 K over a period of 3 ps (3000 time steps), with the temperature being increased by 5 K every 0.05 ps (50 time steps). Initial velocities were assigned on the basis of a Gaussian distribution. Structures were saved every 50 time steps for distance monitoring.

Equilibration. Equilibration of the acyl enzymes was done in two steps. In the first step, structures were equilibrated for a total of 20 ps (20 000 time steps), and the temperature was checked every 0.05 ps (50 time steps). If the temperature was outside of the range 300 ± 10 K, velocities were rescaled by scalar multiplication. The second equilibration followed the same procedure, but temperatures were required to be within a range of ±5 K.

Simulation. Final molecular dynamics trajectories for the simulation phase were conducted for a total of 20 ps. Structures were saved every 0.05 ps (50 time steps). Table II shows average properties for the 400 structures saved during simulation of each

(14) van Gunsteren, W. F.; Berendsen, H. J. C. *Angew. Chem., Int. Ed. Engl.* **1990**, *29*, 992.

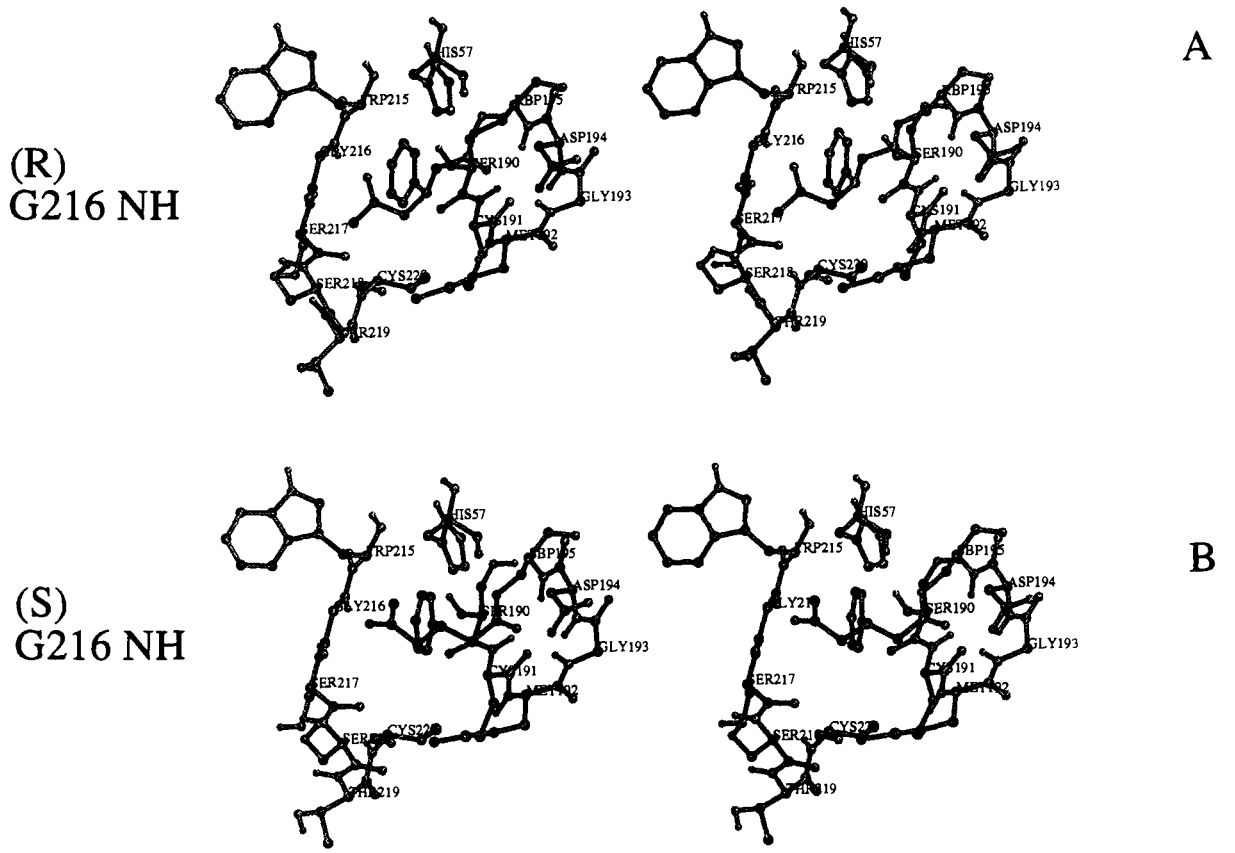

Figure 4. Relaxed stereoscopic view of chymotrypsin acyl enzymes. Top structure A is for *R*/Gly-216 structure, and bottom structure B is for *S*/Gly-216.

acyl enzyme. The first column indicates the stereochemistry of the starting acyl enzyme (i.e., *R* or *S* β-phenyl) and the residue to which the ketone carbonyl is hydrogen bonded in the starting structure (starting structures are those shown in Figure 4). All of the carbonyl-exchanged acyl enzyme structures lost both of the ketone carbonyl/oxyanion hole hydrogen bonds during the heating phase of molecular dynamics. For this reason they were not considered further.

Results of Molecular Dynamics Simulation on Acyl Enzymes. A summary of the geometric rearrangements that the acyl enzymes underwent during the entire 63-ps dynamics run is given in Table III. A plus sign in a column indicates that the hydrogen bond donor/acceptor distance was less than 3.5 Å, while a minus sign indicates that the distance was greater.

Distance Changes. A more in-depth view of the geometric changes that took place during the molecular dynamics run for the *R* β-phenyl acyl enzyme with the ketone carbonyl hydrogen bonded to the Ser-218 OH is given in Figure 5. The first two graphs, A and B, show traces of the distance between the ester carbonyl oxygen and the oxyanion binding hole NH's (Gly-193 and Ser-195) during the heating phase of the run. One can readily see that as the structure is heated from 0 (at 0 ps) to 300 K (at 3 ps), the oxyanion binding hole distances go from less than 3 Å to more than 4.5 Å, the change to Gly-193 occurring before that to Ser-195. In these two graphs we are observing the loss of the hydrogen bonds between the ester carbonyl and the oxyanion binding hole.

Graphs C and D show orientation changes for the ketone carbonyl group during the same 3-ps heating period. Graph C, a plot of the distance between the ketone carbonyl and the Ser-218 OH, shows that this hydrogen bond seems to be *lost* at ca. 2 ps into the run. Concommitant to the loss of the Ser-218 hydrogen bond, a hydrogen bond between the ketone carbonyl and the Gly-216 NH is *formed*. This is illustrated in graph D, which is a trace for the Gly-216 NH to ketone carbonyl distance.

Figure 6, a plot of the ketone carbonyl to Gly-216 NH distance during the simulation phase of the dynamics run, illustrates the stability of the newly formed ketone/Gly-216 hydrogen bond. It is readily observed over the 5-ps time period shown that these groups remain hydrogen bonded, although there are transient excursions to greater separations.

Rather than present distance traces for key geometric parameters for all phases of each dynamics run, we have chosen to summarize the data as follows. The average structure for each phase of the dynamics runs was calculated: For heating, preliminary equilibration, and final equilibration, 100 structures each were used to calculate the averages; for the 20-ps simulation, 100 structures were used to calculate average geometries for each 5-ps segment. Figure 7 shows plots of key distances for the average structures for each segment of the molecular dynamics runs vs time (ps) of completion of each phase. Additionally, distances for the minimized starting structures are included at the 0-ps point.

These figures give a good indication of the time at which the geometric arrangement of the acyl enzymes changed. Distances monitored for each graph are ketone carbonyl oxygen to Met-192 nitrogen, ketone carbonyl oxygen to Gly-216 nitrogen, ketone carbonyl oxygen to Ser-218 OH oxygen, ester carbonyl oxygen to Gly-193 nitrogen (oxyanion hole), and ester carbonyl oxygen to Ser-195 nitrogen (oxyanion hole).

As can be seen from Table III, and from Figure 7, all of the *R* acyl enzymes lost the hydrogen-bonding network formed by the ester carbonyl oxygen and the oxyanion binding hole during the dynamics runs, while only one of the *S* acyl enzymes lost this network. Since the *R* acyl enzymes deacylate much more slowly than the *S* acyl enzymes,[8b] we take these molecular dynamics results as an indication that the retention or loss of the hydrogen bonds between the ester carbonyl oxygen and the oxyanion binding hole NH's is an important factor governing the hydrolytic stability of acyl enzymes. Because the *R* ester carbonyl oxygen is pulled out of the oxyanion binding hole, the deacylation tetrahedral intermediate (**4** from Scheme I) that begins to form as a water molecule attacks this ester will not benefit from hydrogen bonding to the oxyanion binding hole. Therefore, the net effect of the reduced ester/oxyanion binding hole interactions in the *R* acyl enzymes is to raise the energy of activation for attack of water on the acyl enzyme, thereby slowing the deacylation process.

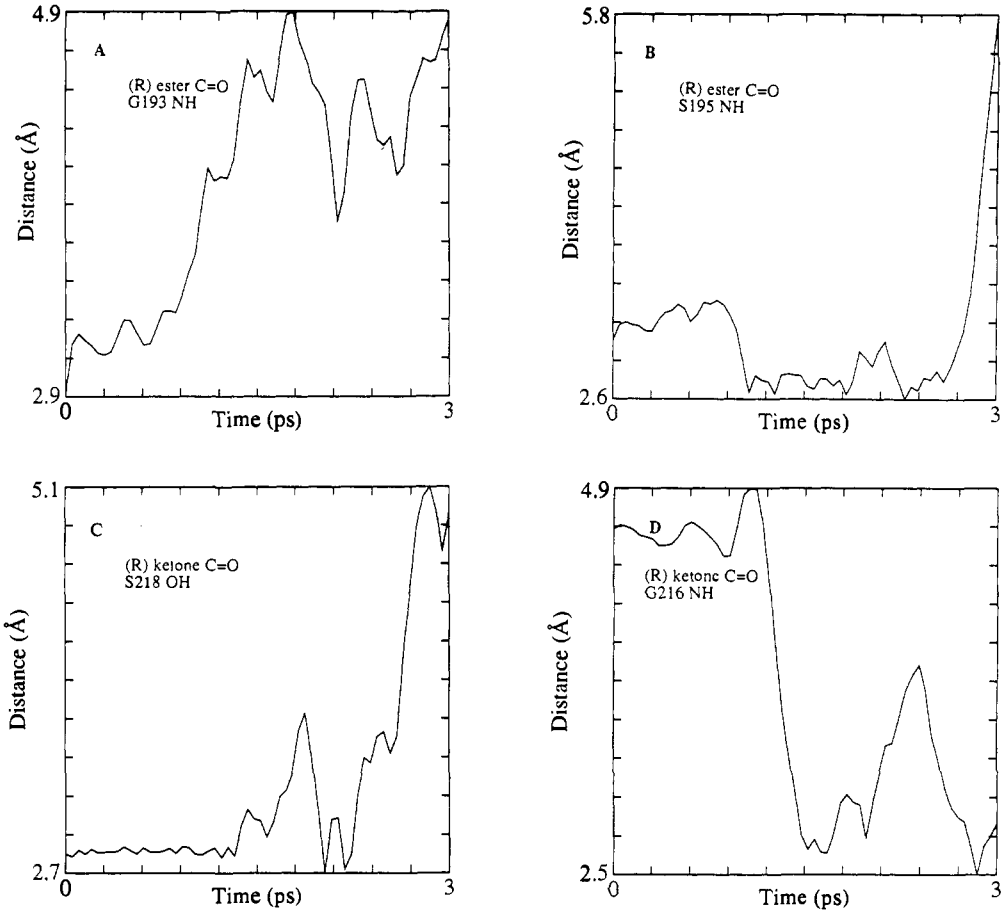

Figure 5. Distance traces for *R*/Ser-218 acyl enzyme during heating portion of molecular dynamics run. Graph A shows distance between ester carbonyl oxygen and Gly-193 nitrogen, graph B shows distance between ester carbonyl oxygen and Ser-195 nitrogen, graph C shows distance between ketone carbonyl oxygen and Ser-218 Oγ, and graph D shows distance between ketone carbonyl oxygen and Gly-216 nitrogen.

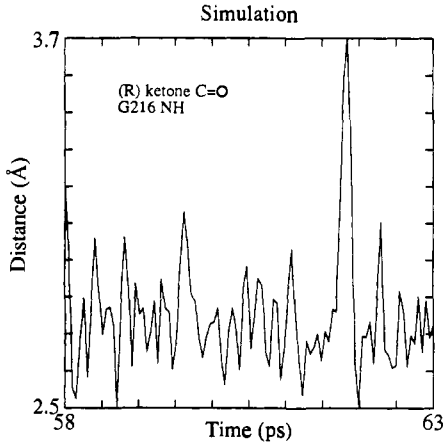

Figure 6. Distance trace for *R*/Ser-218 acyl enzyme during final 5-ps portion of the 20-ps molecular dynamics simulation. Graph shows distance between ketone carbonyl oxygen and Gly-216 nitrogen.

Two of the *S* acyl enzymes have both of the ester/oxyanion binding hole hydrogen bonds intact, and so should hydrolyze normally. The third *S* acyl enzyme, the structure that starts out with the ketone hydrogen bonded to Met-192, loses the oxyanion binding hole hydrogen bonds. It should also be noted that this appears to be a relatively high energy geometry.

The fate of the ketone carbonyl hydrogen bond pair is also interesting. Although the oxyanion ester carbonyl hydrogen bonds are lost in the three *R* acyl enzyme structures, the side chain hydrogen bond persists in the Met-192 NH and Gly-216 NH cases; the Ser-218 OH hydrogen bond switches to Gly-216 NH. With the *S* acyl enzymes, both the side chain Met-192 NH and the Gly-216 cases end up with the acetonyl side chain within hydrogen-bonding distance to both Gly-216 and Ser-218; curiously the *S* acyl enzyme that starts with its acetonyl side chain hydrogen bonded to Ser-218 OH ends up with the hydrogen bond to Gly-216 NH.

Development of Structural Models for Chymotrypsin Deacylation Tetrahedral Intermediates. To study the geometry of the tetrahedral intermediates formed by these acyl enzymes during the deacylation step (**4** in Scheme I), we again relied on molecular dynamics. We built and minimized the tetrahedral intermediates following essentially the same protocol as for the acyl enzymes described earlier. First, we defined new residue topology files for both the *R* and the *S* acylated serine residues. As before, charges were taken from similar RTF's in the CHARMM/quanta database. Because there were no structures electronically similar to oxyanions in the database, we chose to arbitrarily assign a full one-electron charge to the oxyanion oxygen, and to distribute the local effect of the charge as shown in Figure 1.

The ketone carbonyl was placed consecutively within productive hydrogen-bonding distance of the three donors provided by the Met-192 NH, the Gly-216 NH, and the Ser-218 OH. In all structures the phenyl group was placed in the hydrophobic pocket, and the oxyanion was placed, appropriately, in the oxyanion binding hole. In the tetrahedral intermediate, the His-57 imidazole ring is protonated, so we substituted His-57 in our starting structures with the protonated residue Hsc-57 (Hsc is the CHARMM abbreviation for a protonated histidine). Additionally, it was necessary to define new parameters for the HO–C–O^- bending energy, so we used the parameters for the very similar RO–C–OR bond. As with the acyl enzymes, these tetrahedral intermediates were subjected to a sequence of energy minimizations, with the final minimization being completely free of constraints (see above). The results of these minimizations are shown numerically in Table IV, and graphically for the *R* and *S* Gly-216 structures in Figure 8.

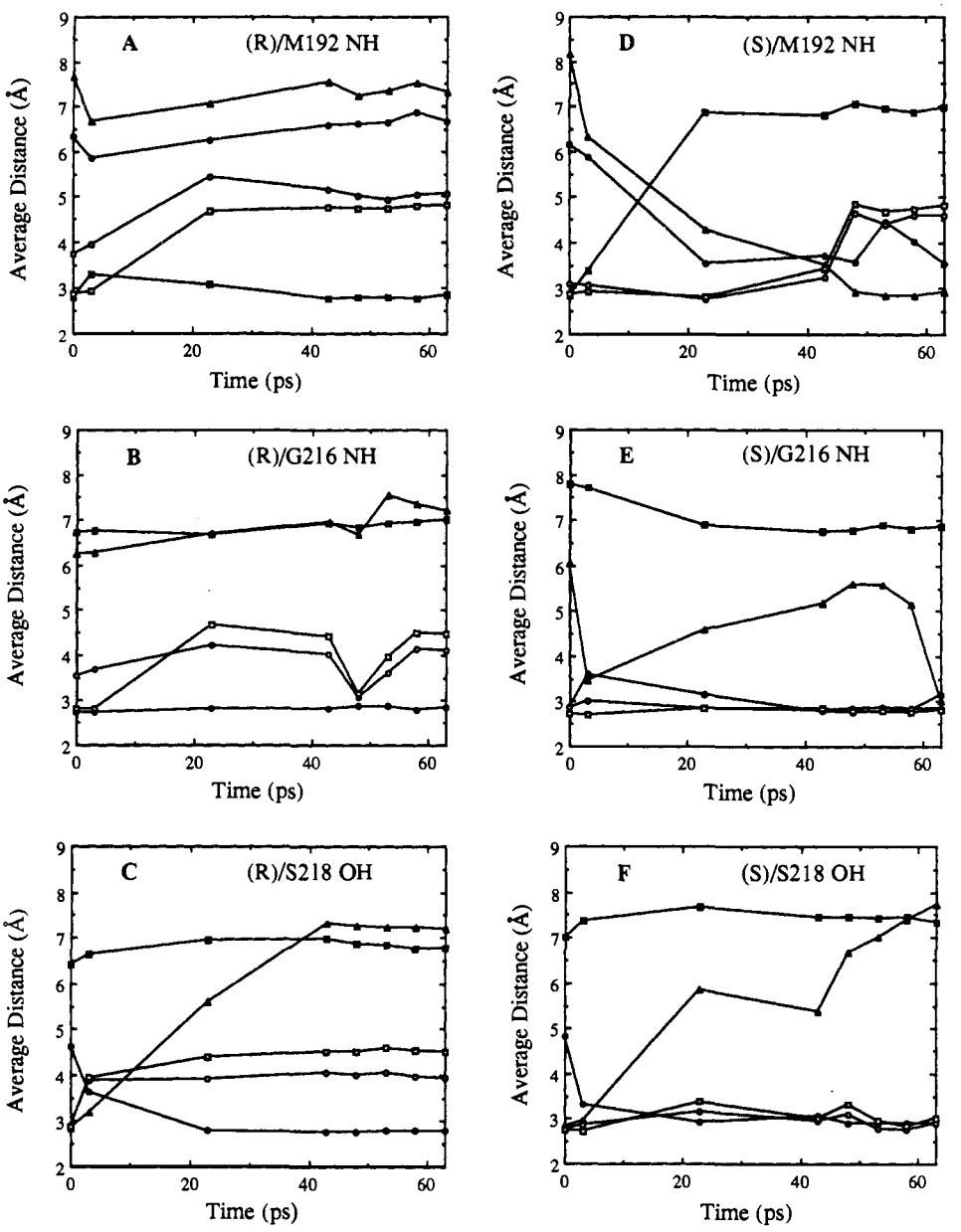

Figure 7. Average distances for key heteroatom separations in acyl chymotrypsins during molecular dynamics run. Panels A–C show plots for *R* acyl enzymes, and panels D–F show plots for *S* acyl enzymes. Panels A and D show average distances for Met-192 NH structures, panels B and E show average distances for Gly-216 NH starting structures, and panels C and F show average distances for Ser-218 OH starting structures. Oxyanion hole distances are represented by hollow figures: ○ for Gly-193 nitrogen to ester carbonyl oxygen distance and □ for Ser-195 nitrogen to ester carbonyl oxygen distance. Ketone carbonyl distances are represented by filled figures: ■ for ketone oxygen to Met-192 nitrogen, ● for ketone oxygen to Gly-216 nitrogen, and ▲ for ketone oxygen to Ser-218 Oγ.

Table IV. Energies and H Bond Distances for Minimized Tetrahedral Intermediates

(stereochem) H bond donor	H bond distance (Å)	minimized energy (kcal/mol)	oxyanion hole distances (Å) Gly-193	Ser-195
(*R*) Met-192 NH	2.89	−5596.2	2.74	2.71
(*R*) Gly-216 NH	2.88	−5558.0	2.70	2.69
(*R*) Ser-218 OH	2.85	−5596.1	2.70	2.75
(*S*) Met-192 NH	2.96	−5590.4	2.67	2.68
(*S*) Gly-216 NH	2.87	−5552.3	2.79	2.66
(*S*) Ser-218 OH	2.85	−5552.8	2.87	2.67

Table V. Averages for 20-ps Dynamics Simulation[a]

ketone H bond starting geometry	av simulatn potentl energy (kcal/mol)	av simulatn total energy (kcal/mol)	av simulatn temp (K)
R Gly-216 NH	−4728.75 (587.09)	−2693.71 (0.94)	304.51 (3.87)
S Gly-216 NH	−4852.80 (547.59)	−2858.17 (0.80)	298.47 (3.64)

[a] Numbers in parentheses are rms values.

Comparison to Acyl Enzymes. As can be seen in Table IV, we were able to form stable structures for all three of the hydrogen-bonding patterns found for the acyl enzymes. By comparing Tables I and IV, the acyl enzymes and their corresponding deacylation tetrahedral intermediates, we can see that the ester carbonyl oxygens in the acyl enzymes form longer and therefore weaker hydrogen bonds to both residues of the oxyanion binding hole (the Gly-193 and Ser-195 NH's) than do the alkoxides of the tetrahedral intermediate. The average oxygen to Gly-193 nitrogen distance goes from 3.15 Å in the six normal acyl enzymes to 2.74 Å in the tetrahedral intermediates. A smaller decrease is seen for the oxygen to Ser-195 nitrogen distance which goes from 2.82 Å in the acyl enzymes to 2.69 Å in the tetrahedral intermediates. These changes are well recognized and are in accord with the concept of catalysis; that is, energy of activation for a reaction is lowered by selective stabilization of the transition state. (In this work, we are using the tetrahedral intermediates

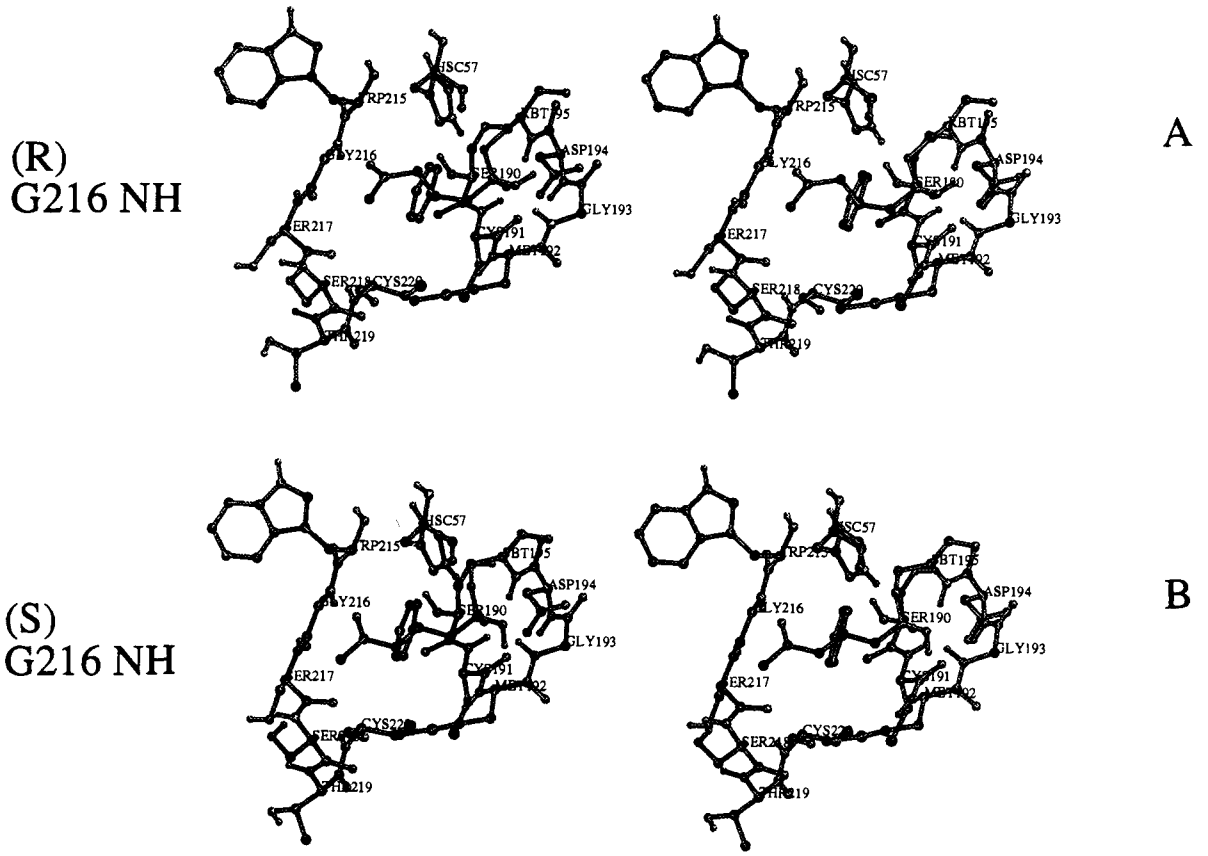

Figure 8. Relaxed stereoscopic view of chymotrypsin deacylation tetrahedral intermediates. Top structure A is for *R*/Gly-216 structure, and bottom structure B is for *S*/Gly-216.

as approximations for the deacylation transition states.)[15]

It is important to compare energies only within a group of similar molecules. This is demonstrated vividly by comparing the energies between acyl enzymes and their corresponding tetrahedral intermediates. Wipff et al. also found that acylation tetrahedral intermediates were lower in energy than the corresponding acyl enzymes and attributed this to increased electrostatic interaction.[6]

Molecular Dynamics on Deacylation Tetrahedral Intermediates. We chose to study the molecular dynamics of the *R* and *S* tetrahedral intermediates having the ketone/Gly-216 hydrogen bond. The importance of these structures can be seen in Tables I–III: For both the *R* and *S* acyl enzymes, the minimized energy of the Gly-216 hydrogen-bonded structures are the lowest (Table I); when the *R* and *S* acyl enzymes are subjected to molecular dynamics simulations, the lowest values for both average potential energy and total energy are found for acyl enzymes that *end up* with the Gly-216 hydrogen bond (Tables II and III).

With these considerations in mind, we heated, equilibrated, and simulated the two tetrahedral intermediates whose starting structures are shown in Figure 8. All of the protocols for the dynamics runs were the same as for those of the acyl enzymes. The average structures for each phase of the dynamics runs for the tetrahedral intermediates were calculated. For heating, preliminary equilibration, and final equilibration, 100 structures each were used to calculate the averages. For the 20-ps simulation, 400 structures were used to calculate the average geometries. Figure 9 shows plots of key distances for the average structures for each segment of the molecular dynamics runs vs time (ps) of completion of each phase. Distances for the minimized starting structures are also included at 0 ps. Distances monitored in each graph are ketone carbonyl oxygen to Met-192 nitrogen, ketone carbonyl oxygen to Gly-216 nitrogen, ketone carbonyl oxygen to Ser-218 OH oxygen, oxyanion oxygen to Gly-193 nitrogen (oxyanion hole), and oxyanion oxygen to Ser-195 nitrogen (oxyanion hole).

Distance Changes. Figure 9A shows that the ketone carbonyl hydrogen bond for the *R* structure moves from Gly-216 to Ser-218, while graph B shows that the *S* structure does not undergo any reshuffling of the same ketone hydrogen bond; in fact, although the *S* structure shows some excursions of the ketone carbonyl hydrogen bonds to Gly-216 and Ser-218, the hydrogen-bonding distances at the end of the simulation are the same as at the start. For both structures, we can see that the oxyanion oxygen/Ser-195 hydrogen bond remains intact. The major difference is in the oxyanion oxygen/Gly-193 hydrogen bond: In the average structure for the 20-ps simulation of the *R* tetrahedral intermediate, this distance is almost 4 Å, but for the *S* tetrahedral intermediate the average is under 3 Å.

We can get a better idea of the differences between the two simulations from Figure 10, which shows detailed traces of the oxyanion oxygen/Gly-193 nitrogen distances for the *R* and *S* tetrahedral intermediates during these 20 ps. It is clear from graph A that in the *R* structure, the distance varies between 2.7 and 4.5 Å, while graph B (note, ordinate scale is smaller) shows that in the *S* structure the distance goes as low as 2.6 Å and rarely ventures above 3 Å. This may be taken as an indication that the *R* tetrahedral intermediate is not as well stabilized by the oxyanion binding hole as the *S* tetrahedral intermediate. Energies and rms deviations for the tetrahedral intermediates during the simulation are shown in Table V.

(15) We have chosen to focus on the different patterns of hydrogen bonding in the *R* and *S* acyl enzymes and tetrahedral intermediates involved in the deacylation process, to provide a rationale for the observed differences in deacylation rates. While we note that the differences in both the static and dynamic energies of the *R* and *S* enantiomers in the acyl enzyme (starting structure) and the tetrahedral intermediate (transition structure mimic) are consistent with the slower rate of deacylation of the *R* enantiomers, we hesitate to place much weight on these quantitative differences. They are much larger than expected, and as we noted, there was also a considerable difference in the average temperatures during the dynamics simulations of the enantiomers of the two tetrahedral intermediates (Table V). Also, as noted by a reviewer, deacylation rates could be affected by factors in addition to hydrogen bonding, namely, by steric factors involved in the attack of water or by differences in the nucleophilicity of the attacking water resulting from alterations in the catalytic triad.

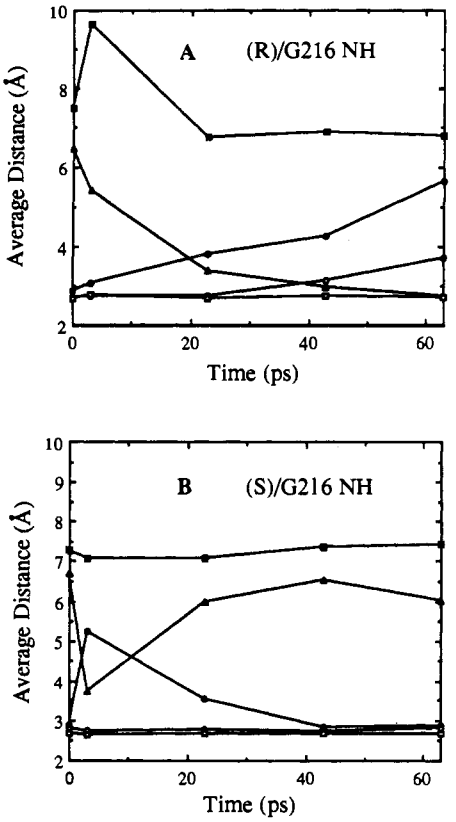

Figure 9. Average distances for key heteroatom separations in chymotrypsin deacylation tetrahedral intermediates during molecular dynamics run. Panels A and B show plots for *R* and *S* tetrahedral intermediates starting from Gly-216 NH starting structures. Oxyanion hole distances are represented by hollow figures: ○ for Gly-193 nitrogen to oxyanion distance and □ for Ser-195 nitrogen to oxyanion distance. Ketone carbonyl distances are represented by filled figures: ■ for ketone oxygen to Met-192 nitrogen, ● for ketone oxygen to Gly-216 nitrogen, and ▲ for ketone oxygen to Ser-218 Oγ.

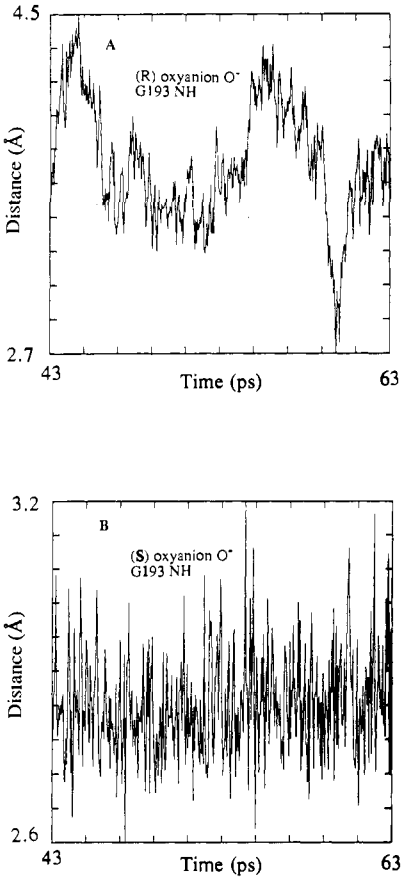

Figure 10. Distance traces A and B for *R* and *S*/Gly-216 tetrahedral intermediates during 20-ps molecular dynamics simulation. Graphs show distance between oxyanion and Gly-216 nitrogen.

Although it is tempting to compare the average potential energies for the simulations and point out that the *R* structure is much less stabilized than the *S*,[15] one must keep in mind that this energy difference may be due to the 6.0 K temperature difference between the average simulation temperatures. Comparisons of this sort are much more valid in cases such as the dynamics runs from Table II, where the average temperatures only span a range of 2.5 K for all six structures. The addition of a longer equilibration period for both *R* and *S* tetrahedral intermediates, before simulation, could possibly lead to energy values that would be more quantitative. The most important features for these simulations, however, are the hydrogen-bonding changes that go on in the oxyanion binding hole and in the ketone carbonyl hydrogen bond.

Conclusion

The molecular dynamics studies presented here have provided us with a new understanding of serine protease deacylation rates, specifically for the *R* and *S* β-phenyl acyl enzymes **8** and **7**. We have seen how a combination of factors involving hydrogen bonding of the ketone carbonyl and the ester carbonyl conspire to slow the deacylation rate of the *R* acyl enzyme by a factor of ca. 60 relative to the *S* acyl enzyme. Additionally, we have ruled out the carbonyl-exchanged acyl enzyme hypothesis on the basis of dynamic simulation of those acyl enzymes. An idea that seemed reasonable at 0 K (molecular mechanics alone) was quickly ruled out at 300 K (molecular dynamics). Our current understanding of the differential deacylation rates of **7** and **8** is as follows: Both acyl enzymes have their ketone carbonyls hydrogen bonded to the Gly-216 NH. This is suggested by comparison of static and dynamic energies for all of the acyl enzymes discussed. Both acyl enzymes start out with their ester carbonyl oxygens hydrogen bonded to the Gly-193 NH and the Ser-195 NH, but the *R* acyl enzyme quickly loses both of these hydrogen bonds, as shown graphically in Figure 7. Attack of water to form the deacylation tetrahedral intermediate take place with an activation energy largely determined by stabilization of the newly created oxyanion. Since the *R* acyl enzyme must form an oxyanion that is not well stabilized in this manner, attack of water is an infrequent event, so that the *R* acyl enzyme has a slow deacylation rate (k_d = 0.0029 min^{-1}). In contrast to the *R* case, the *S* acyl enzyme has an ester carbonyl fully hydrogen bonded to both oxyanion binding hole NH's, so the oxyanion formed by attack of water is immediately stabilized; the activation energy for deacylation is lower than for the *R* case, so the *S* acyl enzyme has a faster rate of deacylation (k_d = 0.17 min^{-1}).[15] Additional information is provided by the molecular dynamics studies of the tetrahedral intermediates formed during the deacylation process. Our studies showed that the *R* tetrahedral intermediate lost one of the crucial oxyanion hole hydrogen bonds *even when we started from an idealized structure* with optimal oxyanion hole hydrogen bonds (i.e., not from the tetrahedral intermediate that would initially be formed on the basis of our dynamics runs for the *R* acyl enzymes).

It should now be possible to use molecular dynamics calculations similar to those described above to predict the relative stabilities of acyl enzymes formed by structurally related compounds.[8c]

Acknowledgment. We are grateful for support of this research through grants from the National Institutes of Health (PHS 5RO1 DK27526). Dr. Klaus Schulten and his research group provided us with helpful advice on the molecular dynamics method. Dr. Garland Marshall and Dr. Shungi Naruto introduced us to modeling of serine protease active sites and proposed the carbonyl-exchanged acyl enzymes. Part of the computational work was performed on work stations in the Molecular Graphics Facility (Biotechnology Center, University of Illinois) and the National Science Foundation National Center for Supercomputing Applications (University of Illinois).